Infrared reflectivity probing of thermal and spatial properties of laser-generated carriers in germanium

M. I. Gallant* and H. M. van Driel
Department of Physics and Erindale College, University of Toronto, Toronto M5S 1A7, Canada
(Received 14 December 1981)

We report on the thermal and spatial properties of laser-generated carriers in single-crystal intrinsic germanium as determined from infrared (10.6 μm) reflectivity studies. Densities up to 5×10^{19} cm^{-3} are achieved using fundamental (1.06 μm) and second-harmonic (0.53 μm) 80-nsec pulses from a Q-switched Nd:glass laser. The carriers are probed using a 10.6-μm 100-μsec CO_2 laser beam which is electronically synchronized to the glass laser. For a carrier density of $\sim10^{19}$ cm^{-3}, characteristic of the plasma resonance at 10.6 μm, the reflectivity attains a minimum value; for higher carrier densities the reflectivity is enhanced beyond its intrinsic value (0.36) to values as high as 0.95, depending on the peak surface density. Such transient, laser-induced changes in the reflectivity of semiconductors were first investigated by Galkin and co-workers, who interpreted the reflectivity minimum value in terms of damping of the plasmon resonance by carrier-assisted free-carrier absorption processes. Subsequently Vakhnenko and co-workers offered an interpretation solely in terms of spatial inhomogeneity of the laser-generated carriers. Here we report detailed experimental and theoretical investigations of this transient reflectivity phenomenon in which we have determined the influence of excitation laser wavelength and intensity, lattice temperature, plasma inhomogeneity effects, and surface quality. For a density of $\sim10^{19}$ cm^{-3} our results indicate that intervalence-band absorption and phonon-assisted free-carrier absorption are the dominant damping mechanisms of the plasmon resonance and that spatial inhomogeneity of the carrier density plays a minor, albeit measurable, role in determining the value of the reflectivity minimum. The applications of these results to diagnostics of laser-induced semiconductor plasmas, including pulsed laser annealing and the performance of laser-activated semiconductor reflection switches, are discussed.

I. INTRODUCTION

Infrared reflectivity and transmission have traditionally been very useful tools for the determination of properties of uniformly doped semiconductors, providing information on the carrier density, effective mass, and scattering times.[1–4] The presence of large carrier densities in semiconductors can substantially alter the dielectric coefficient in the infrared and thereby alter the reflectivity and transmission spectrum. For free-carrier densities of $\lesssim10^{20}$ cm^{-3}, the infrared reflectivity undergoes an anomalous dispersion and tends to unity when the incident light frequency approaches the plasmon frequency. The characeteristics of the reflectivity spectrum and, in particular, the value of the reflectivity minimum can be used to determine the carrier properties.

In 1968 Galkin *et al.*,[5] in pioneering work, observed the free-carrier plasma resonance for high-density, laser-generated electrons and holes in intrinsic Ge, Si and GaAs. A high-intensity, 40-nsec pulse from a 0.69-μm ruby laser was used to generate the transient plasma and the plasma was probed in reflection using a 10.6-μm beam from a pulsed, synchronized CO_2 laser. The ruby laser, through band-to-band absorption, generated a rapidly changing carrier density with the constant-wavelength probe effectively scanning the density-dependent plasma resonance. For a 10.6-μm probe the reflectivity minimum occurs for a density of $N_c\simeq1\times10^{19}$ cm^{-3}. The observed reflectivity minimum values for Ge (0.29) and GaAs (0.18) were 0.07 and 0.12 below the intrinsic reflectivity values, respectively, whereas the actual minimum was not observed for Si. In the absence of any damping of the plasmon resonance, the theoretical value of the reflectivity minimum is zero, corresponding to the dielectric coefficient having a

value of 1. The nonzero values observed were said to be associated with strong carrier-assisted free-carrier absorption. Stated differently, the plasmon resonance was considered to be damped by carrier-carrier scattering. Later, Vakhnenko and Strizhevskii[6] reinterpreted the minimum values solely in terms of spatial inhomogeneity of the density of the plasma. In general, a nonzero value of the reflectivity can occur, even in the absence of absorption, if the plasma is inhomogeneous, since light is reflected from different layers and it is not possible to satisfy the condition of zero reflection for all such layers simultaneously. Although these authors offered a quantitative explanation for the minimum reflectivity, the carrier diffusion coefficient (3 cm^2/sec) and carrier lifetime ($\sim 10^{-11}$ sec) used by them to justify the existence of a 0.2-μm-thick plasma are much lower than the usually accepted values of 65 cm^2/sec[7] and 50 nsec,[8] respectively, at least in the case of germanium for a density of N_c.

Since carrier-carrier scattering is generally not the most important mechanism in determining the carrier relaxation time in ambipolar plasmas[9] and due to the inappropriate material parameters used by Vakhnenko and Strizhevskii, we seriously doubted the interpretations offered. In view of the potential use of infrared reflectivity in probing the properties of high-density plasmas in semiconductors and its possible use as a diagnostic tool in pulsed laser-annealing processes, we have performed a detailed characterization of the transient reflectivity phenomenon including the dependence on excitation wavelength and intensity, lattice-plasma temperature, carrier-density inhomogeneity and surface preparation. These studies have enabled us to identify the important plasmon resonance-damping mechanisms and to determine the influence of density inhomogeneity and carrier-lattice temperature. A preliminary report of some aspects of this work was published elsewhere.[10] Besides the applications cited above, the results presented here are of importance to the development of laser-activated semiconductor reflection switches and ultrashort infrared pulse generation.[11]

We will divide the remainder of this paper into five parts. In Sec. II we present a theoretical model and numerical results for the generation and evolution of carrier density and the lattice-plasma temperature during pulsed laser interactions with germanium. Section III will briefly consider the theoretical reflectivity of homogeneous and inhomogeneous carrier distributions. Section IV gives the experimental technique used in obtaining our results, with the results and interpretations offered in Sec. V. Lastly, the results are summarized in Sec. VI.

II. PULSED LASER INTERACTION WITH GERMANIUM: CARRIER GENERATION AND HEATING

The absorption of pulsed laser radiation by semiconductors leads to the creation of nonequilibrium carrier densities and elevated carrier and lattice temperatures. How much of the laser photon energy is partitioned into electron-hole pairs, carrier kinetic energy, phonons, etc., is a very active area of research and is obviously dependent on the time scale over which information is sought. In the work discussed here we are interested in situations where 10^{-7}-sec pulses, with peak power densities of 10^7 W/cm^2, interact with the semiconductor. Under these conditions it is generally acknowledged[10,12] that the carrier and lattice temperatures are essentially the same (the carrier temperature will be slightly higher than the lattice temperature in the region of carrier generation, but for the situations considered here this difference is less than 25 K). The plasma can therefore be characterized by two macroscopic quantities, namely, its density and temperature. The temporal and spatial evolution of the carrier density and carrier-lattice temperature are governed by diffusion equations. Because the material properties including the diffusion coefficients are temperature dependent, the two equations have to be solved simultaneously. This approach has been used by a considerable number of researchers to model the interactions of nsec pulses with semiconductors. There are, however, two important aspects of the carrier diffusion process which have not been incorporated to date. The first involves the induced band bending of the semiconductor as a result of an inhomogeneous temperature. Because the band gap of most semiconductors decreases with increasing temperature, the band gap will be lowest near the surface, where the temperature is highest. Brown[13] originally pointed out that this effect could present barriers to the normal diffusion process and we have recently shown[14] that in extreme situations diffusion will not occur at all, with the plasma being confined near the surface. The other process is the thermoelectric effect whereby carriers are driven by

a temperature gradient. This effect, which we have also considered in our recent work,[14] would ordinarily enhance the diffusion process but in general it is weaker than the effect related to the band bending.

With the above comments in mind, in the absence of any applied electric fields, the electron-hole pair current density can be written as[14]

$$\vec{J}=-D\left[\vec{\nabla}N+\frac{N}{2k_BT}\vec{\nabla}E_g+\frac{N}{2T}(p+p'+2)\vec{\nabla}T\right], \quad (1)$$

where D is the ambipolar diffusivity, N is the electron-hole pair density, E_g is the energy gap, T is the carrier-lattice temperature, and p and p' are defined by the kinetic energy (E_k) dependence of the carrier scattering times τ. For electrons, $\tau_e \propto E_k^p$ with a similar expression determining the hole exponent p' in $\tau_h = E_k^{p'}$. For carrier-phonon interactions $p=p'=-\frac{1}{2}$. As will be demonstrated in this paper, even at high densities the carrier relaxation time is determined by carrier-phonon interactions, so this is the only case we will consider in the present calculation. The value of D and its temperature dependence are consistent with this assumption. In Eq. (1) the first term is the diffusion current density, the second term results from the force field associated with spatial variations of the band edge, and the third term represents the contribution from the thermoelectric effect. It has implicitly been assumed that the carrier distributions are nondegenerate, with the result that for $T>300$ K there is no density dependence of the diffusivity. For some of the densities and temperatures considered, the assumption of nondegeneracy is marginal, but we estimate that even in the worst case the value of D is no more than 20% larger than the value assumed. This has only a small effect on the calculated carrier densities and lattice temperatures.

Equation (1) can be simplified if one assumes that the spatial variation of the band gap is due to variations of the lattice temperature only. The band gap also decreases as a result of many-body effects such as carrier exchange and correlation,[15] but for the densities considered here the reduction of the band gap through thermal effects is much more important. Assuming (reasonably) that the band gap decreases linearly with temperature above 300 K, with temperature coefficient $r=-k_B^{-1}(\partial E_g/\partial T)$, Eq. (1) becomes

$$J=-D\left[\vec{\nabla}N+\frac{N}{2T}(p+p'+2-r)\vec{\nabla}T\right]. \quad (2)$$

The evolution of the carrier density can be determined through the equation of continuity, which is given by

$$\vec{\nabla}\cdot\vec{J}+\frac{\partial N}{\partial t}=\frac{I(t)(1-R)\alpha e^{-\alpha x}}{\hbar\omega}-\gamma N^3, \quad (3)$$

where we have considered the pairs to be generated at a depth x through band-to-band absorption by a pulse of intensity $I(t)$ and photon energy $\hbar\omega$, impinging at normal incidence on a semiconductor of reflectivity R and absorption coefficient α. In our experiments we have used photon energies of 1.17 eV (1.06 μm) and 2.34 eV (0.53 μm) which exceed not only the indirect gap E_g (0.67 eV at 300 K) but also the direct energy gap (0.80 eV), so that strong absorption occurs near the semiconductor surface. Carrier recombination at high densities is taken to occur via an Auger process with recombination coefficient γ. Equations (2) and (3) can be combined to give the density diffusion equation,

$$\frac{\partial N}{\partial t}=\vec{\nabla}\cdot\left[D\vec{\nabla}N+\frac{N}{2T}(p+p'+2-r)\vec{\nabla}T\right]+\frac{I(t)(1-R)\alpha e^{-\alpha x}}{\hbar\omega}-\gamma N^3. \quad (4)$$

The values of the material parameters and their temperature dependence for $300<T<1000$ K are given in Table I.

Equation (4) can be solved in the usual one-dimensional approximation subject to the boundary condition

$$N(x\rightarrow\infty,t)=N_i,\qquad D\left.\frac{\partial N}{\partial x}\right|_{x=0}=S(N-N_i), \quad (5)$$

where $N_i\simeq 10^{13}/\text{cm}^3$ is the intrinsic equilibrium carrier density and S is the surface recombination velocity, which depends on surface conditions. The value of S ranges from $\sim 10^2$ cm/sec for polished and chemically etched surfaces to $\sim 10^6$ cm/sec for mechanically polished (abraded) surfaces. Because of the lattice-temperature dependence of the material parameters and the $\vec{\nabla}T$ term, Eq. (4) must be solved simultaneously with an equation which describes the evolution of the

TABLE I. Material parameters for germanium.

Parameter	Value	Reference
R (0.53 μm)	0.50	16
R (1.06 μm)	0.39	16
R (10.6 μm)	0.36	17
α (1.06 μm)	$1.4\times10^{4}(1+T/2000)$ cm^{-1}	20
α (0.53 μm)	$5\times10^{5}(1+T/3600)$ cm^{-1}	20
D	$65(T/300)^{-1.5}$ cm^{2}sec^{-1}	17,18
C	$1.7(1+T/6000)$ JK^{-1}cm^{-3}	19
γ	2×10^{-31} cm^{6}sec^{-1}	8
D_L	$0.35(T/300)^{-1.1}$ cm^{2}sec^{-1}	17

carrier-lattice temperature. In formulating this equation we will assume that the electron-hole pairs instantaneously lose their excess energy $[\hbar\omega-E_g-2(\frac{3}{2}k_BT)]$, imparted to them in the absorption process, so that the effective heat generation depth is α^{-1}. There has been some discussion in the literature[21] concerning carrier diffusion effects allowing the heat generation depth to be larger than α^{-1}, but for the 80-nsec pulses considered here this is not important since, on this time scale, the temperature spatial dependence is not very sensitive to the value of the depth chosen.[22] The thermal diffusion equation can therefore be written in the form[12]

$$\frac{\partial T}{\partial t}=\frac{\partial}{\partial x}\left[D_L\frac{\partial T}{\partial x}\right]+\frac{\alpha(1-R)I(t)e^{-\alpha x}}{C}\left[\frac{\hbar\omega-E_g-3k_BT}{\hbar\omega}\right]+\frac{\gamma N^3}{C}(E_g+3k_BT)\,, \tag{6}$$

where C is the specific heat and D_L is the lattice thermal diffusivity. The electronic contribution to the thermal diffusivity is negligible for the densities of interest. Heat generation via the Auger recombination process has been included, in which the energy $E_g+2(\frac{3}{2}k_BT)$ lost by the recombining electron-hole pair is given to a third carrier and therefore immediately to the lattice. This term is less than 20% of the other heat generation term for the maximum carrier densities considered here. Other heat generation processes, such as loss of carrier energy during band-gap reduction, are too insignificant to be considered here. On a nsec time scale little heat is lost from the surface. On the other hand, heat is generated at the surface if the surface recombination velocity is different from zero. Equation (6) must therefore be solved subject to the boundary conditions

$$K_T\frac{\partial T}{\partial x}+S(N-N_i)(E_g+3k_BT)=0\,,\qquad T(x\to\infty)=300\text{ K}\,, \tag{7}$$

where K_T is the thermal conductivity.

We have simultaneously solved Eqs. (4) and (6) together with their boundary conditions using standard finite difference techniques. Figure 1 shows the carrier-density profiles which occur at different times during the excitation of a $S=0$ sample by Gaussian (in time) 80-nsec, 1.06-μm pulses of incident peak power density 1 and 2 MW/cm^2. The curves correspond to the times at which the carrier density at the surface reaches the value of N_c, the surface density of principal interest in this paper. Since the surface density can essentially follow the excitation pulse, these two times occur when the instantaneous power density is $\sim$0.2 MW/cm^2. These curves change insignificantly for values of S up to $\sim10^4$ cm/sec. For higher values of S, significant deviations can occur. The inset to Fig. 1 shows the corresponding carrier-density profiles obtained for a surface recombination of 5×10^5 cm/sec. For the 1-MW/cm^2 pulse the critical density is just achieved, so that only one curve is shown. Of particular interest in all three curves is that the density initially increases away from the surface as it must in general according to Eq. (5). For all the curves the characteristic profile depth is determined approximately by how far the carriers can diffuse during their Auger lifetime of $\tau_A\sim50$ nsec. This distance is $\sim(D\tau_A)^{1/2}=18$ μm. The actual differences between the shapes of the curves, apart from surface

recombination effects, are related to the extent to which lattice heating will influence the material parameters and also cause band-gap reduction near the surface. This accounts for the steeper profiles exhibited by the d curves, which correspond to the termination of the higher intensity pulse.

Figure 2 shows the corresponding lattice and carrier temperature profiles for the same pulses at the same times in the pulse corresponding to the curves in Fig. 1. It is apparent that for the $S=0$ case there is little lattice heating at the time N_c is reached at the surface for the first time for either pulse. However, a rise in temperature of 75 and 210 K is achieved on the trailing edges of the 1- and 2-MW/cm^2 pulses, respectively. The corresponding lattice temperature curves for $S=5\times10^5$ cm/sec are shown in the inset. The lattice temperatures achieved at the surface are considerably higher than those depicted in the main figure since, with a higher value of S, more recombination occurs. The characteristic profile depths are all ~2 μm, much smaller than the value of the density profile characteristic depth, reflecting the fact that $(D_L/D)^{1/2}\sim0.1$.

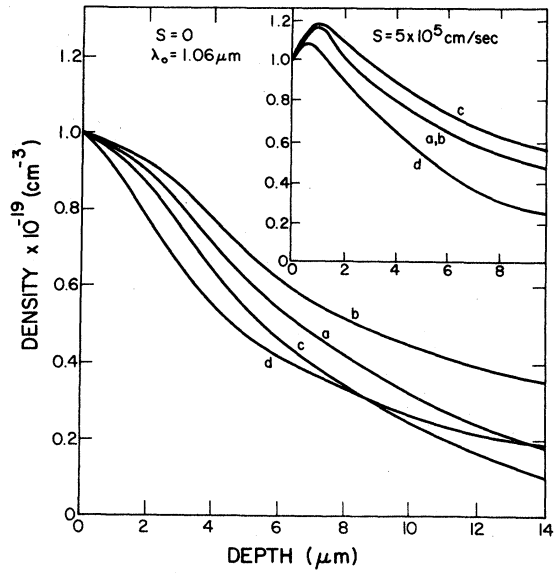

FIG. 1. Carrier-density profiles in germanium for surface recombination velocities of 0 and 5×10^5 cm/sec and 1.06-μm illumination. The a and b curves are associated with the leading and trailing edges of a 80-nsec 1-MW/cm^2 Gaussian pulse when the surface density is 10^{19} cm^{-3}. Curves c and d are associated with a 2-MW/cm^2 pulse.

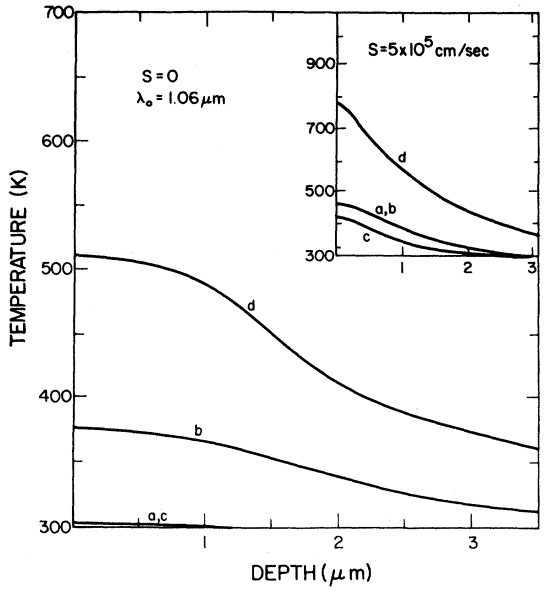

FIG. 2. Lattice temperature profiles associated with the carrier-density profiles shown in Fig. 1.

For 0.53-μm illumination, higher incident intensities must be employed to achieve the same density because the sample reflectivity is higher and more of the laser's photon energy is used to heat the carriers. Figures 3 and 4 show the carrier-density and lattice temperature profiles for 2- and 4- MW/cm^2 pulses. All of the curves for the density depict much shallower profiles since in general higher lattice temperatures are achieved. For the largest temperature gradient (curves d in Fig. 4), a significant degree of carrier confinement is apparent in the corresponding density profile. The factor of 30 difference in the absorption coefficients for 0.53 and 1.06 μm intrinsically has little influence on the calculated profiles, as can be seen in those cases in which lattice heating is small.

III. INFRARED REFLECTIVITY FROM HOMOGENEOUS AND INHOMOGENEOUS CARRIER DISTRIBUTIONS

The optical reflectivity and transmissivity of any material are determined as functions of frequency by the complex dielectric function $\epsilon(\omega)$. For infrared frequencies which are below that associated with the fundamental absorption edge the dielectric function can be highly dispersive due to the presence of free carriers. The Drude model for free

carriers has been successfully used for describing the optical properties of extrinsically doped semiconductors[1] after quantum corrections associated with intervalence-band absorption have been made. With this combined classical and quantum model, for a plasma with equal numbers of electrons and holes the real (ϵ_R) and imaginary (ϵ_I) parts of $\epsilon(\omega)$ can be written in cgs units as

$$\epsilon_R(\omega)=\epsilon_\infty-4\pi Ne^2\left[\frac{1}{m_e^*}\left\langle\frac{\tau_e^2}{1+\omega^2\tau_e^2}\right\rangle+\frac{1}{m_h^*}\left\langle\frac{\tau_h^2}{1+\omega^2\tau_h^2}\right\rangle\right]+4\pi\chi_{iV}\,,$$

$$\epsilon_I(\omega)=\frac{4\pi Ne^2}{\omega}\left[\frac{1}{m_e^*}\left\langle\frac{\tau_e}{1+\omega^2\tau_e^2}\right\rangle+\frac{1}{m_h^*}\left\langle\frac{\tau_h}{1+\omega^2\tau_h^2}\right\rangle\right]+\frac{4\pi\sigma_{iV}}{\omega}\,, \tag{8}$$

where $\epsilon_\infty=16$ is the intrinsic high-frequency dielectric constant, $m_{e,h}^*$ is the electron or hole optical effective mass, $\tau_{e,h}$ is their momentum relaxation time, and χ_{iV} and σ_{iV} are the susceptibility and conductivity associated with intervalence-band absorption. Averages over the carrier energy distribution indicated by the $\langle\ \rangle$ brackets can be transferred to the carrier relaxation times with negligible error.[23] For germanium, $m_e^*=0.12m_e$, $m_h^*=0.23m_e$, and $4\pi\sigma_{iV}/\omega=4\times10^{-19}\,N$ cm^3 for $\lambda=10.6$ μm.[24] The corresponding susceptibility in this wavelength region is negligible compared to the free-carrier susceptibility.

The complex dielectric function determines the complex refractive index whose real (n) and imaginary (κ) parts are given by

$$2n^2=\epsilon_R+(\epsilon_R^2+\epsilon_I^2)^{1/2}\,,$$
$$2\kappa^2=-\epsilon_R+(\epsilon_R^2+\epsilon_I^2)^{1/2}\,. \tag{9}$$

From the values of n and κ the normal incidence reflectivity at an air-semiconductor interface of a semi-infinite semiconductor can be found from Fresnel's equation,

$$R=\frac{(n-1)^2+\kappa^2}{(n+1)^2+\kappa^2}\,. \tag{10}$$

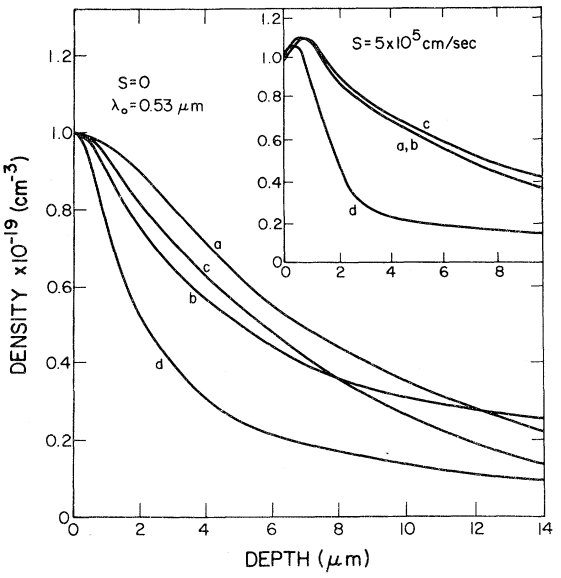

FIG. 3. Similar to Fig. 1 except the a and b curves are associated with a 2-MW/cm^2 0.53-μm pulse, and the c and d curves are associated with a 4-MW/cm^2 0.53-μm pulse.

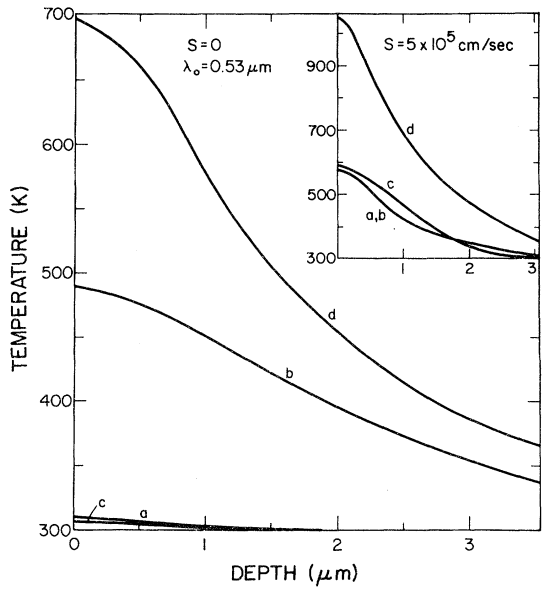

FIG. 4. Lattice temperature profiles corresponding to Fig. 3.

For negligible damping ($\omega\langle\tau_{e,h}\rangle \gg 1$ and $\sigma_{iV} \simeq 0$) the value of κ is small and $n \simeq \epsilon_R^{1/2}$. In this case the real part of the refractive index will vanish if the carrier density is such that the plasmon frequency equals the probing frequency; i.e.,

$$\omega = \omega_p = \left[\frac{4\pi N_p e^2}{\epsilon_\infty} \left[\frac{1}{m_e^*} + \frac{1}{m_h^*} \right] \right]^{1/2}, \quad (11)$$

where N_p is the carrier density corresponding to the plasmon frequency ω_p. If $n = \kappa \simeq 0$, then $R = 1$. At a slightly lower density, $N_c = [(\epsilon_\infty - 1)/\epsilon_\infty]^{1/2} N_p$, we have $n = 1$, $\kappa \simeq 0$, and $R = 0$. For $\omega\langle\tau_{e,h}\rangle \gtrsim 1$ and/or large σ_{iV} the plasmon resonance will be damped with $\kappa \neq 0$ and the minimum value of R is different from zero. Since σ_{iV} is known, the value of the reflectivity minimum is determined by the value of the carrier scattering time.

In intrinsic materials there are basically only two mechanisms which determine this time, namely carrier-carrier and carrier-phonon processes. At least for low densities, it is well known that for $T > 300$ K the carrier scattering time is determined by optical- and acoustic-phonon scattering. For electrons at room temperature acoustic-mode scattering is approximately four times stronger than optical-mode scattering, while the reverse is approximately true for holes.[25] Above room temperature intervalley scattering becomes important for electrons, leading to a significant influence on the value of $\langle\tau_e\rangle$. In any event, to the extent that it is meaningful to define a relaxation time for either type of carrier when optical-phonon or intervalley scattering occurs, it has been determined[18,26] that above room temperature $\langle\tau_e\rangle = 3\times10^{-13}(T/300)^{-2.5}$ sec and $\langle\tau_h\rangle = 3\times10^{-13}(T/300)^{-3.0}$ sec for germanium. At room temperature the intervalence-band contribution to ϵ_I dominates, whereas at $T \simeq 1000$ K the free-carrier part dominates.

For large, excess carrier densities carrier-carrier scattering has often been suggested as being important in determining the carrier scattering time. Indeed, as already indicated, Galkin and coworkers, in the interpretation of their experiments on laser-induced plasmas in germanium, considered that the damping of the plasma resonance was due entirely to carrier-carrier interactions. Using the Conwell-Weiskopf formula for impurity scattering, modified to deal with degenerate electron-hole scattering,[27] they determined theoretically that at room temperature $\langle\tau_{e,h}\rangle \sim 10^{-14}$ sec. The application of the Conwell-Weiskopf formula to germanium is inappropriate, however, for at least two reasons. First, at $N = N_c$ the carrier distributions are not degenerate since the quasi-Fermi-levels are essentially within $k_B T$ of the band edges. More importantly, in an ambipolar plasma in the absence of an applied electric field, the electrons and holes diffuse together with the same average velocity, whereas in the case of impurity scattering the carriers scatter from essentially stationary impurities. Meyer[28] has recently pointed out in a theoretical paper that for ambipolar carrier flow the effect of carrier-carrier scattering on the diffusivity is very small and does not significantly affect the carrier scattering time as determined by lattice scattering. In any event, since for the Boltzmann carrier distributions the carrier-carrier scattering time has a $T^{3/2}$ temperature dependence, it will be easy experimentally to determine the relative importance of the two scattering mechanisms from the temperature dependence of the reflectivity minimum.

In Fig. 5 we show two theoretical plots for the normal incidence reflectivity at 10.6 μm as a function of carrier density. The graphs illustrate the expected behavior at $T = 300$ and 900 K for the case in which carrier-lattice scattering and intervalence-band absorption are the plasma resonance damping mechanisms. With an increase in temperature of 600 K the reflectivity minimum shifts from 0.21 to 0.32. In arriving at the two curves indicated we have included the temperature dependence of the high-frequency dielectric constant which arises as a result of the temperature dependence of the band gap. The temperature dependence of ϵ_∞ at $\lambda = 10.6$ μm is given by[29]

$$\epsilon_\infty = [4.0 + 3\times10^{-4}(T - 300)]^2, \quad (12)$$

where T is in Kelvin. This gives an intrinsic reflectivity of 0.36 at 300 K and 0.38 at 900 K. If the reflectivity minimum of 0.21 at 300 K were assumed to be due to carrier-carrier scattering only, the corresponding reflectivity value at 900 K would have decreased to ~ 0.08, a substantially different result.

The above treatment of the reflectivity leading to the results shown in Fig. 5 has assumed that the plasma of carriers is homogeneous. As illustrated in Figs. 1 and 3, carriers generated by pulsed laser absorption are spatially inhomogeneous due to absorption, diffusion, and lifetime effects. In addition, due to laser heating the material properties are also spatially inhomogeneous. If the optical

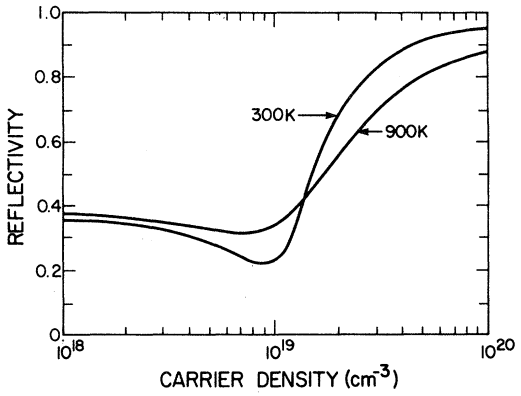

FIG. 5. Theoretical reflectivity characteristic at 10.6 μm if the plasmon resonance is damped by intervalence-band and phonon-assisted free-carrier absorption.

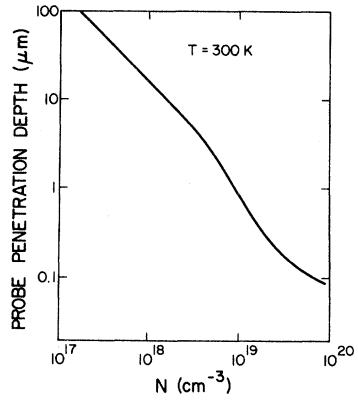

FIG. 6. 10.6-μm probe penetration depth as a function of carrier density.

probe depth is comparable to the distance over which the dielectric function changes, then the Fresnel formula is no longer applicable for calculating the reflectivity. In Fig. 6 we show how the probe depth $c(2\kappa\omega)^{-1}$ varies with carrier density for $\lambda=10.6$ μm. For the critical density N_C the probe depth is less than 1 μm, so that in most cases spatial inhomogeneity effects will be small. The main exception occurs if S is high, in which case the density varies rapidly in the vicinity of the surface.

The reflectivity of optically inhomogeneous materials can, of course, be treated using the characteristic matrix method for stratified media,[30] but if the dielectric function has an analytical dependence on depth, the reflectivity may be obtained more easily from the direct solution of Maxwell's equations. This has been done for the particular case of inhomogeneous carrier distributions in semiconductors by Subashiev and Kukharskii[31] and Vakhnenko and Strizhevskii.[6] Situations in which the dielectric function varies linearly or exponentially with depth yield direct analytic results for the reflectivity; more complex functional dependences must be treated numerically. With the results of Figs. 1 and 3 in mind, for simplicity we will assume that the density varies exponenentially with depth. Ignoring for the moment temperature effects, one can assume that the depth (x) dependence of the dielectric function is of the form

$$\epsilon(x)=\epsilon_B-\beta e^{-x/\delta}\,, \tag{13}$$

where ϵ_B is the bulk dielectric function, and β and δ are defined through the actual carrier distributions. For the case where $S=0$ we can approximate $N(x)$ by $N_0e^{-x/\delta}$ with $N_0=N_C$. It follows that $\epsilon_B=\epsilon_\infty$ and β can be determined from Eq. (8). For $S=5\times10^5$ cm/sec we can approximate $N(x)$ by $N_0'-\Delta Ne^{-x/\delta}$ with $N_0'\simeq N_C$, $\Delta N/N_0'\sim0.2$, and ϵ_B and β determined from Eq. (8). Although in the limit of $x\to\infty$ this latter expression gives $N\to N_0'$, contrary to Figs. 1 and 3, over an effective probing depth of $\lesssim1$ μm the expression can be used to represent the density profile. From Figs. 2 and 4 it might be argued that one should take into account inhomogeneities in $\epsilon(\omega)$ as contributed by the temperature dependence of $\langle\tau_{e,h}\rangle$. Owing to the functional dependence of ϵ on $\langle\tau_{e,h}\rangle$, incorporation of this inhomogeneity would be formidable. However, for most of the cases of interest to us, $\omega\langle\tau_{e,h}\rangle>1$, and ϵ_R is only weakly dependent on $\langle\tau_{e,h}\rangle$ while the free-carrier part of ϵ_I is smaller than the intervalence-band component. Thermal inhomogeneities, at least for surface temperatures of $T\lesssim800$ K, can be expected to be small.

In general, for ϵ as given by Eq. (13) the reflectivity can be written as

$$R=\left|\frac{\rho_0-\psi}{1+\psi}\right|^2\,, \tag{14}$$

for

$$\rho_0=\frac{1-\sqrt{\epsilon_B}}{1+\sqrt{\epsilon_B}}\,,\qquad \psi=\frac{J_{-\nu+1}(i\zeta)}{J_{-\nu}(i\zeta)}\frac{\sqrt{\beta}}{\sqrt{\epsilon_B}+1}\,, \tag{15}$$

where $J_\alpha(\ )$ is the Bessel function of the first kind of order α. The argument is defined through

$$\zeta=\frac{2\omega\delta}{c}\sqrt{\beta}\,, \tag{16}$$

and the orders of the Bessel functions are found from

$$\nu=\frac{2\omega i\sqrt{\epsilon_B}\delta}{c} . \tag{17}$$

Figure 7 shows the dependence of the reflectivity minimum at 10.6 μm as a function of δ for situations in which the density decreases away from the surface ($S=0$) and increases away from the surface ($S\neq 0$). In all cases the surface density is assumed to be N_C and the material parameters used in the graphs are the same as those for the $T=300$ K curve in Fig. 5. In Fig. 7, curve *a* shows the reflectivity minimum at a constant value of 0.21 as obtained from a homogeneous plasma, curve *b* represents the $S=0$ case, while curves *c* and *d* illustrate $N/N_0'=0.2$ and 0.5, respectively, with $S=5\times 10^5$ cm/sec. Over a broad range of δ it can be seen that if the density decreases away from the surface, the reflectivity minimum values are larger than those of the homogeneous case, whereas if the density increases, lower reflectivity values would be seen. In either case, as $\delta\rightarrow 0$ the reflectivity values approach those appropriate to the value of $\epsilon(\omega)=\epsilon_B$, whereas as $\delta\rightarrow\infty$ the reflectivity approaches the value appropriate to $\epsilon(\omega)=\epsilon_B-\beta$. The oscillations in the reflectivity near $\delta\simeq 0.2$ μm are characteristic of interference effects.

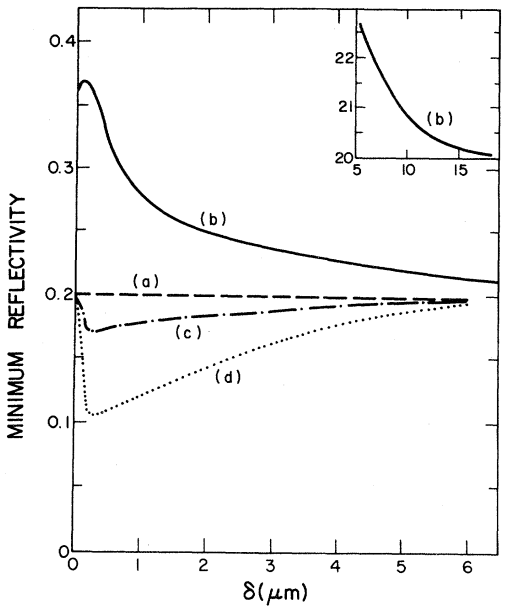

FIG. 7. Minimum reflectivity at 10.6 μm from inhomogeneous plasmas. Curve *a* labels a particular reflectivity for a homogeneous plasma. Curve *b* indicates the case where the plasma density decreases exponentially away from the surface with characteristic depth δ, while *c* and *d* show the behavior if the density increases exponentially away from the surface with the asymptotic bulk density being 20% (curve *c*) and 50% higher than the surface value.

IV. EXPERIMENTAL DETAILS

A schematic diagram of the experimental arrangement used to measure the 10.6-μm reflectivity of laser-generated plasmas in germanium is shown in Fig. 8. A *Q*-switched Nd:glass laser is used in multimode operation to produce 80-nsec-wide gaussian pulses at 1.06 μm with a peak power of 5 MW. A second harmonic beam at 0.53 μm is generated with about 5% conversion efficiency in a KD*P crystal for some of the experiments. The probe beam is derived from a 1-kW CO_2 laser which produces multimode pulses of $\sim$75-μsec duration. The glass and CO_2 lasers are electronically synchronized so that the *Q*-switched pulse occurs near the peak of the 10.6-μm pulse. Because of the 10^3 factor difference in pulse widths, the 10.6-μm pulse is essentially cw (continuous wave) during the 1.06- and 0.53-μm pulse. The laser beams are directed and focused onto a 400-μm-thick germanium slab. The germanium samples used in the experiments were nominally intrinsic

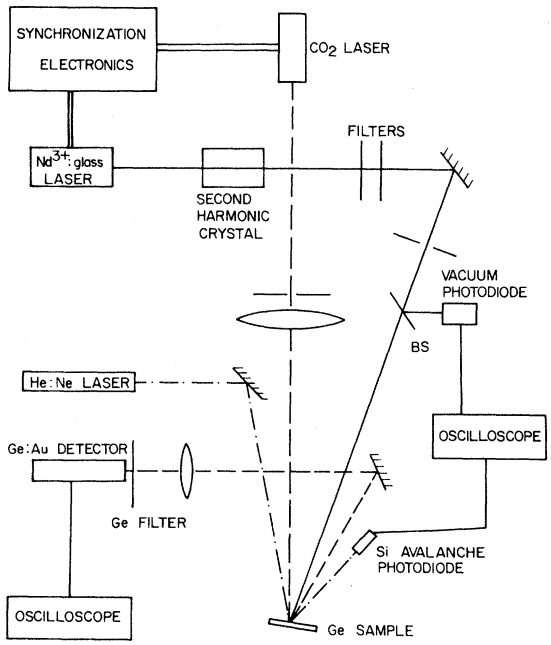

FIG. 8. Experimental schematic.

single crystals with a room-temperature resistivity of 20 Ω cm. They were mechanically polished on one side and some were chemically etched using various acid etches. The other side of the sample was purposely roughened so as to prevent a second reflecting interface for the 10.6-μm beam. In those experiments designed to measure the influence of lattice temperature of the reflectivity, the sample was heated directly using a dc current source. Sample temperatures up to ~ 750 K were measured by a copper constantan thermocouple mounted within 3 mm of the illuminated spot on the sample.

The excitation and probe beams overlap on the sample, with the diameter of the 10.6-μm spot being $\frac{1}{4}$ of the 5-mm spot size of the 1.06- and 0.53-μm beam. Filters were used to control the intensities of the two beams. In particular, the power density of the CO_2 laser beam was kept below 10^2 W/cm^2 so as not to induce any lattice heating itself. The angle of incidence of the probe beam is about 5° off normal and the reflected beam is detected with a fast Ge:Au detector. A thick piece of germanium is used in front of the detector to block 0.53- and 1.06-μm light. The signal from the detector is amplified using a DC-3 GHz amplifier and displayed on a Tektronix 7633 storage oscilloscope. The overall response time of the system is 3 nsec. The excitation beam is monitored using a F4000 ITT vacuum photodiode coupled to a Tektronix 7904 oscilloscope. The energy of the excitation pulse is measured using a Joulemeter with the peak power density determined by the beam-spot size at the sample. The uncertainty in the power density is estimated to be $\pm 20\%$.

For experimental expediency, the full duration of the Q-switched pulse was used, so that from one pulse variable density plasmas were generated as a function of time, thereby scanning the plasma reflectivity minimum depicted in Fig. 5. For sufficiently high excitation pulses the resonance is scanned on the leading and trailing edges of the pulse. Experiments were conducted varying the spot size and location of the probe beam within the 1.06-μm spot to test overlap and homogeneity, with no significant change in the results unless the spot sizes were comparable. In order to check for damage or melting during excitation, a 0.633-μm He-Ne beam was used in reflection to monitor the sample, with the reflected beam detected by a Si avalanche photodiode. For the maximum laser power density used (~ 17 MW/cm^2), the maximum possible carrier density prior to sample melting, according to the formalism in Sec. II, is $\sim 8\times 10^{19}$ cm^{-3}, corresponding to a plasmon resonance of ~ 3.8 μm. Therefore any changes in the 0.633-μm beam can be interpreted only in terms of sample damage or melting effects and not due to a plasma resonance.

V. EXPERIMENTAL RESULTS AND DISCUSSION

Measurements of the infrared reflectivity of laser-excited plasmas in germanium were carried out under a wide variety of excitation-laser intensities, sample surface conditions and sample temperatures.

Figure 9 shows the typical reflectivity at 10.6 μm observed from an etched germanium sample with a 1.0-MW/cm^2 1.06-μm excitation pulse. The figure is reproduced from an oscilloscope photograph. On the same figure the profile of the excitation pulse is indicated as well. The reflectivity of the probe beam is taken to be 0.36 (corresponding to $\epsilon_\infty = 16$) before the excitation pulse strikes the sample. This number is therefore used as a reference in converting the oscilloscope traces to actual reflectivity values at each point in time. It can be seen that the reflectivity initially decreases to a value of 0.21, rises to a peak of 0.7, and decreases to a second minimum of 0.22. The two minima occur at the two points in the excitation pulse where the instantaneous intensity is ~ 0.2 MW/cm^2, corresponding to a surface density of carriers equal to N_C. The slow recovery of the re-

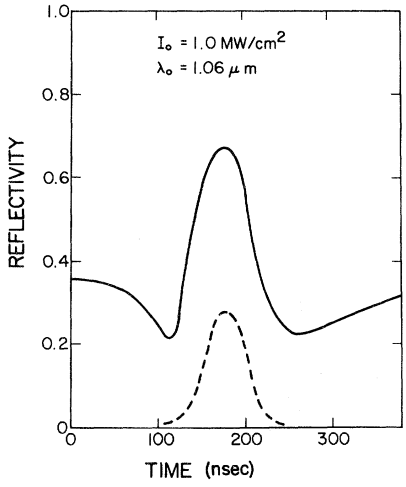

FIG. 9. Typical recorded reflectivity trace at 10.6 μm (solid line) for a 1.06-μm 1-MW/cm^2 pulse. The dashed line indicates the profile of the excitation pulse.

flectivity following the final minimum can be attributed to the density-dependent Auger recombination lifetime of $\tau_A \gtrsim 50$ nsec. The fact that the two minima do not have exactly the same value is consistent with laser heating of the lattice. The maximum reflectivity value of 0.70 is consistent with the maximum carrier density achieved, namely 2×10^{19} cm^3.

Figure 10 depicts the reflectivity observed as a function of time for pulses of different peak excitation intensity up to 2 MW/cm^2. Except for the lowest intensity case, which shows only a single minimum, the other traces indicate two minima, with the value of the first minimum being 0.21 in each case. For each peak intensity, the increase in surface temperature is calculated to be not more than 10 K at the time of the first minimum and it is not surprising that the initial reflectivity minimum does not change. The second minima show higher values for pulses of peak intensity greater than $\sim$0.75 MW/cm^2. For the 1- and 2-MW/cm^2 pulses the surface temperatures are calculated to be 375 and 510 K, respectively, at the time of the second minimum. The actual reflectivity values are 0.22 and 0.26, both of which are in good agreement with the theoretical values of 0.21 and 0.24 if one assumes damping of the plasmon resonance by intervalence-band absorption and phonon-assisted free-carrier absorption. The residual difference between theory and experiment for these minima as well as the initial minimum value of 0.21 (theoretical value 0.20) can be explained from plasma inhomogeneity. From Figs. 1 and 7 with $\delta\simeq12$ μm, the difference of $\sim$0.01 is easily explained. An interesting case occurs if the peak intensity is between 0.2 and $\sim$0.75 MW/cm^2. The second minimum reflectivity has a value which is slightly ($\sim$0.005) lower than the first minimum. For intensities less than 0.75 MW/cm^2 the temperature rise at the time of the second minimum is less than 40 K. However, as illustrated by the *a* and *b* curves of Fig. 1, for $S=0$ the curve corresponding to the density profile on the trailing edge of the pulse shows less carrier inhomogeneity than the corresponding curve on the leading edge of the pulse. As a result of representing a more homogeneous plasma, it is not surprising that the second minimum value is lower than the first.

At intensities much higher than 2 MW/cm^2 new structure is observed in the reflectivity signature. Figure 11 shows the reflectivity traces for probe wavelengths of 10.6 and 0.63 μm for a peak excitation of 8 MW/cm^2. The oscillation in the 10.6-μm reflectivity near the peak is always correlated with a rise in the 0.63-μm reflectivity by $\sim$0.10. This is believed to be due to melting of the sample surface at 1185 K and subsequent resolidification. This would account for the drop of the 10.6-μm reflectivity near the peak since the reflectivity of molten germanium[30] is $\sim$0.7. The fact that this value is not actually attained for either beam is similar to an observation by Auston *et al.*[32] on laser-irradiated silicon. We will not pursue this point further here. The reflectivity minimum

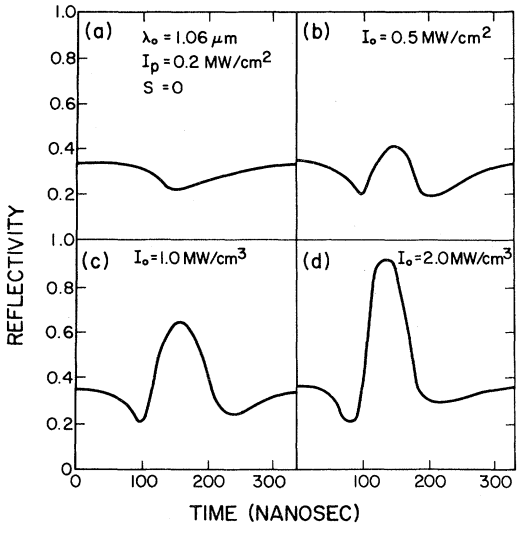

FIG. 10. Reflectivity traces for 10.6 μm for an etched sample for excitation pulse power densities between 0.2 and 2 MW/cm^2.

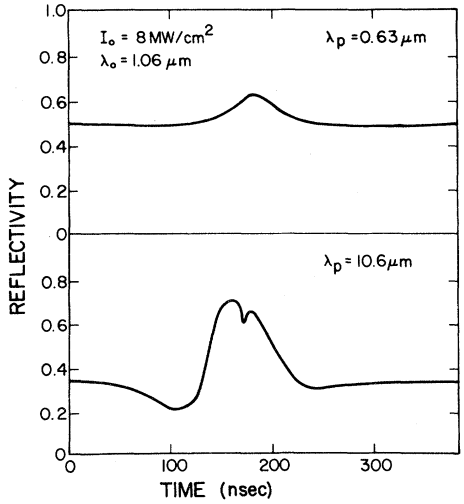

FIG. 11. Reflectivity traces for 0.63 and 10.6 μm as produced by an 8-MW/cm^2 1.06-μm excitation pulse.

value of ~ 0.32 which occurs on the trailing edge of the pulse is consistent with a sample temperature near melting, assuming the intervalence-band and phonon-assisted free-carrier absorption model.

In order to directly compare our model with the models of Galkin *et al.* and Vakhnenko and Strizhevskii for the reflectivity minimum, we uniformly heated the sample directly with a dc current source and recorded the values of the first reflectivity minima associated with 1-MW/cm^2 excitation. The maximum temperature rise induced by the pulse at the time of the first minimum is less than 10 K. The reflectivity minima were recorded for six different sample temperatures between 300 and 750 K, with the results shown in Fig. 12. Also shown are the predicted temperature dependences of the three different models. For germanium at room temperature, Galkin had measured a minimum reflectivity value of 0.29 and attributed this to a room-temperature carrier-carrier scattering time of 10^{-14} sec. The intensity at the time of the first minimum was 10^{25} photons/cm^2, corresponding to an intensity of 3 MW/cm^2 at 0.69 μm. The prediction of his theory is that the reflectivity minima would decrease rapidly with increasing temperature. This clearly does not fit the data.

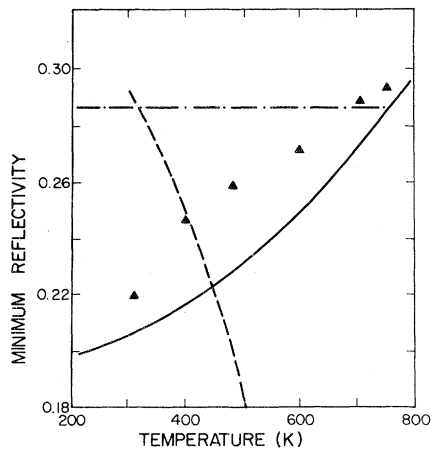

FIG. 12. Experimental data (▲) for the dependence of the 10.6-μm reflectivity minimum on the lattice temperature for a directly heated sample. The — · — line is the theoretical prediction based on spatial inhomogeneity of the plasma density, the — — — line is based on damping of the plasmon resonance by carrier-assisted free-carrier absorption, while the solid line is indicative of damping of the plasmon resonance by intervalence-band and phonon-assisted free-carrier absorption in a homogeneous plasma.

The theory based on spatial inhomogeneity effects used to explain the data of Galkin *et al.* at $T=300$ K has no intrinsic temperature dependence and so also does not fit the data. On the other hand, the theory which incorporates phonon-assisted free-carrier and intervalence-band absorption accounts for the data rather well, although, as noted earlier, the theory underestimates the data. Part of this discrepancy, 0.01, can be attributed to optical inhomogeneity effects for a carrier-density profile with a depth $\delta \sim 12$ μm. Beyond this, the discrepancy has to be considered good, considering the approximations involved in the Drude model and possible inhomogeneity effects associated with ϵ_∞ and $\langle \tau_{e,h} \rangle$. We suggest that the value of $R=0.29$ measured by Galkin *et al.* is associated with strong heating effects at his intensity.

The results depicted thus far indicate that density inhomogeneities serve only a minor role in the optical properties of laser-generated plasmas, at least under the conditions considered. However, the effect of the spatial inhomogeneity may not be completely negligible in all situations. A preliminary account of our work[10] indicated that for mechanically polished, unetched samples the initial reflectivity minima were lower than those reported here for etched samples, whereas the intensities needed to attain those minima were much higher. If one did not take into account the actual surface conditions, there would be a temptation to interpret the lower reflectivity minima in terms of $\langle \tau_{e,h} \rangle$ or σ_{iV}. Figure 13 shows the reflectivity minima achieved for etched and coarsely polished, unetched samples for peak excitation intensities of 0.2- and 1-MW/cm^2 1.06-μm pulses, respectively. The fivefold increase in intensity is indicative of a much larger surface recombination, as is the more rapid return to the 0.36 reflectivity value. The increase in excitation intensity for the unetched sample is consistent with a surface recombination of $S \simeq 5 \times 10^5$ cm/sec, which prompted this choice of S for our analysis in Sec. II. For the unetched sample the reflectivity minimum value of ~ 0.18 is ~ 0.04 lower than for the etched sample. This lower value is consistent with the density increasing away from the surface with $\delta \sim 1$ μm and $\Delta N/N_0' \simeq 0.2$, as indicated in Fig. 1, and the theoretical reflectivity minimum of ~ 0.17, as predicted by Fig. 7. The residual discrepancy can be accounted for by sample heating effects or a slightly different value of $\Delta N/N_0'$. Our theoretical analysis also indicates that for $S=5 \times 10^5$ cm/sec the carrier lifetime near the surface is $\lesssim 10$ nsec,

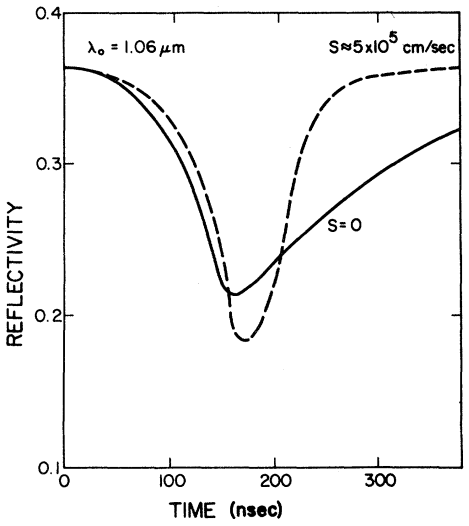

FIG. 13. Reflectivity traces at 10.6 μm for unetched and etched samples at peak excitation power densities of 0.2 and 1.0 MW/cm^2, respectively.

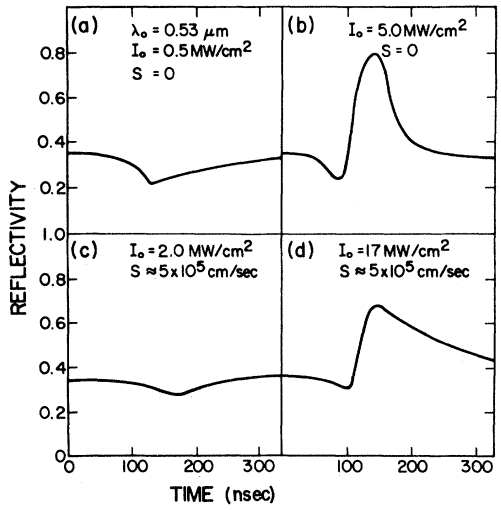

FIG. 14. Reflectivity traces produced by 0.53-μm excitation pulses at different intensities for etched and unetched samples.

so the reflectivity would return to its equilibrium value following the profile of the excitation pulse.

Finally, to illustrate the role of excitation wavelength, Fig. 14 shows the 10.6-μm reflectivity of germanium irradiated with 0.53-μm pulses for intensities up to 17 MW/cm^2 and for etched and unetched samples. Again, it can be observed that for the etched samples the initial reflectivity minima are independent of peak excitation level and their value, $R \simeq 0.21-0.22$, is only marginally, if at all, higher than the initial reflectivity minimum for 1.06-μm illlumination. This can be understood with the aid of Fig. 4 which indicates that the surface temperature has risen by less than 20 K at the time of the first minimum. For peak power densities between 0.5 and 5 MW/cm^2 the second reflectivity minimum increases monotonically from 0.21 to 0.36, similar to the 1.06-μm-excitation case. However, as seen from Fig. 14(b), for a peak power density of 5 MW/cm^2 a second minimum is not actually observed. This can be accounted for by the density and temperature profiles shown in Figs. 3 and 4 which indicate steep profiles and high lattice temperatures. From Fig. 7 the reflectivity minima are expected to be ~ 0.05 higher than those of the homogeneous case for $\delta \sim 3$ μm. However, these comments should only be interpreted semiquantitatively since, with both high temperatures and spatial inhomogeneity effects present, the relative importance of the two effects to increasing the reflectivity minimum is not clear. Further work on this phenomenon is in progress. Figures 14(c) and 14(d) show the corresponding results for the unetched samples at two excitation intensities. An intensity of ~ 2 MW/cm^2 is required to attain the minimum reflectivity and its value of ~ 0.26 is consistent with an estimated temperature of 600 K. The influence of carrier inhomogeneity effects is perhaps masked by the large thermal effect. At 17 MW/cm^2 the initial minimum reflectivity (~ 0.26) is consistent with a temperature of ~ 600 K at this point. The second minimum is absent most likely for the same reasons as those offered for Fig. 14(b). The longer recovery time to equilibrium is explainable by the longer cooling time required at the higher excitation level.

VI. SUMMARY

We have shown that a considerable amount of detailed information about the properties of photogenerated, high-density plasmas in semiconductors can be obtained from a study of their infrared reflectivity. We have clearly shown that the increase in lattice temperature that accompanies plasma excitation has a marked influence on the properties of the plasma. In addition we have shown that intervalence-band absorption and carrier-phonon scattering are the dominant plasmon resonance

damping mechanisms and that carrier-carrier scattering and optical inhomogeneity effects are small for etched samples. The latter effect on the infrared reflectivity is most apparent if the surface recombination velocity is high enough that the carrier-density profile is inhomogeneous within a skin depth of the surface.

ACKNOWLEDGMENTS

We gratefully acknowledge the financial support of the Natural Sciences and Engineering Research Council of Canada in these investigations. One of us (M.I.G.) is grateful to the Province of Ontario for a scholarship.

---

*Present address: Bell Northern Research, Ottawa, Ontario, Canada.

[1]W. G. Spitzer and H. Y. Fan, Phys. Rev. 106, 883 (1957).

[2]J. I. Pankove, in *Progress in Semiconductors,* edited by A. F. Gibson and R. E. Burgess (Heywood, London, 1976), Vol. 9, p. 67.

[3]H. Y. Fan, in *Semiconductors and Semimetals,* edited by R. K. Willardson and A. C. Beer (Academic, New York, 1967), Vol. 3, p. 406.

[4]D. I. Bilenko, A. A. Kukharskii, V. K. Subashier, and V. D. Tsiporuka, Fiz. Tekh. Poluprovodn. 6, 1170 (1972) [Sov. Phys.—Semicond. 6, 1028 (1972)].

[5]G. N. Galkin, L. M. Blinov, V. S. Vavilov, and A. G. Golaushkin, Zh. Eksp. Teor. Fiz. Pis'ma Red. 7, 93 (1968) [JETP Lett. 1, 69 (1968)].

[6]I. F. Vakhnenko and V. L. Strizhevskii, Fiz. Tekh. Poluprovodn. 3, 1844 (1969) [Sov. Phys.—Semicond. 3, 1562 (1970)].

[7]S. M. Sze, *Physics of Semiconductor Devices* (Wiley, New York, 1971).

[8]D. H. Auston, C. V. Shank, and P. LeFur, Phys. Rev. Lett. 35, 1022 (1975).

[9]J. Appel, Phys. Rev. 125, 1815 (1961); J. R. Meyer, Phys. Rev. B 21, 1554 (1980).

[10]P. C. Hein, M. I. Gallant, and H. M. van Driel, Solid State Commun. 39, 601 (1981).

[11]A. J. Alcock, P. B. Corkum, and D. J. James, Appl. Phys. Lett. 27, 680 (1975); S. A. Jamison, A. V. Nurmikko, and H. J. Gerritsen, *ibid.* 29, 640 (1976); A. J. Alcock and P. B. Corkum, Can. J. Phys. 57, 1280 (1979).

[12]H. M. van Driel, T. L. F. Leung, and M. I. Gallant Phys. Rev. B (unpublished); E. J. Yoffa, *ibid.* 21, 2415 (1980); J. R. Meyer, F. T. Bartoli, and M. R. Kruer, *ibid.* 21, 1559 (1980); A. Elci, M. O. Scully, A. L. Smirl, and J. C. Matter, *ibid.* 16, 191 (1977); J. M. Liu, R. Yen, M. Kurz, and N. Bloembergen, Appl. Phys. Lett. 39, 755 (1981).

[13]W. L. Brown, in *Laser and Electron Beam Processing of Materials,* edited by C. W. White and P. S. Peercy, (Academic, New York, 1980), p. 22.

[14]H. M. van Driel, J. S. Preston, and M. I. Gallant, Appl. Phys. Lett. 40, 385 (1982).

[15]W. F. Brinkman and T. M. Rice, Phys. Rev. B 7, 1508 (1973); H. M. van Driel and J. F. Young, J. Phys. C 15, L31 (1982).

[16]R. F. Potter, Phys. Rev. 150, 562 (1966).

[17]N. Neuberger, *Handbook of Electronic Materials* (IFI/Plenum, New York, 1971), Vol. 5.

[18]E. M. Conwell, *High Field Transport in Semiconductors,* (Academic, New York, 1967).

[19]P. Sommelet and R. L. Orr, J. Chem. Eng. Data 11, 1966.

[20]W. C. Dash and R. Newman, Phys. Rev. 99, 1151 (1955).

[21]E. J. Yoffa, Phys. Rev. B 21, 2415 (1980).

[22]R. F. Wood, Appl. Phys. Lett. 38, 357 (1980).

[23]P. A. Schumann, Jr. and R. P. Phillips, Solid State Commun. 10, 943 (1967).

[24]W. Kaiser, R. J. Collins, and H. Y. Fan, Phys. Rev. 91, 1380 (1953).

[25]W. A. Harrison, Phys. Rev. 104, 1281 (1956).

[26]O. A. Golikova and A. V. Petrov, Fiz. Tverd. Tela. 6, 3065 (1964) [Sov. Phys.—Solid State 6, 2443 (1965)]; O. A. Golikova, B. Ya. Moizhes, and A. G. Orlow, *ibid.* 4, 3482 (1962) [*ibid.* 4, 2550 (1963)].

[27]N. H. Fletcher, Proc. IRE 45, 862 (1957).

[28]J. R. Meyer, Phys. Rev. B 21, 1554 (1980).

[29]T. Tsay, B. Bendow, and S. Mitra, Phys. Rev. B 8, 2688 (1973).

[30]M. Born and E. Wolf, *Principles of Optics* (Pergamon, New York, 1975), p. 57.

[31]V. K. Subashiev and A. A. Kukharshii, Phys. Status Solidi 23, 447 (1967).

[32]D. H. Auson, J. A. Golovchenko, A. L. Simons, C. M. Surko, and T. N. C. Venkatesan, Appl. Phys. Lett. 34, 777 (1979).